

A generalized electron transport model in photodetectors for high-speed imaging

T Kundu and D Misra

Department of Electrical and Computer Engineering, New Jersey Institute of Technology, University Heights, Newark, NJ 07102-1982, USA

E-mail: dmisra@njit.edu

Received 17 March 2005, in final form 31 August 2005

Published 26 September 2005

Online at stacks.iop.org/SST/20/1122

Abstract

Photoelectron transport in a photodetector in an ultra-high frame rate image sensor under the uniform illumination condition is investigated. The charge readout time in a multi-implant photodetector is estimated using a generalized model with both diffusion equation and continuity equations. The maximum effective diffusion length was assigned to each implanted region after taking into account the fringing field drift due to multiple implants. Assuming that the charge on each section is directly proportional to its area under uniform illumination, the total charge transport as a function of time is obtained by the superposition of charge contribution of all implanted regions. By increasing the number of implants in the photodetector it may be possible to collect more than 10 million frames s^{-1} . The design effects are also investigated. The model showed excellent match with experimental results.

1. Introduction

Sensitive imaging applications such as optical wave front measurements, study of particles during an explosion and hypersonic gas turbulence image acquisition at a frame rate much higher than 50/60 Hz are required for consumer applications. The sub-microsecond time resolution for these applications requires capturing images at the rate of 10^6 – 10^7 frames s^{-1} . Image sensors with an ultra-high frame rate (10^6 frames s^{-1} or higher) were developed for studying the rapid mechanical motion and transient phenomena [1–3]. It is, therefore, required to collect the photoelectrons consistent with high frame rates. To ensure the maximum number of photoelectrons collection, an efficient design of the photodetector is required. The layout of a micro pixel of such an ultra-high frame rate imager is shown in figure 1. The photodetector generates the charge and the charge is moved to micro pixel memory at a very high speed during the frame acquisition mode through a buried charge coupled device channel. In addition to the photodiode the micro pixel consists of a collection gate G1, antiblooming gate G2, a drain D, a charge transfer gate G3 and a parallel register of a 12-pixel element for immediate storage in the form of a vertical array. It is important to ensure that the photo carriers drift towards the deepest potential point around G1. The operation is critical

in optimizing the detector response time of the imager by obtaining the complete charge readout in much less than 1.0 μs . The optimal design for the detector with a transit time in sub-microsecond regime can be achieved if electrons are mostly drifted in the photodetector to the collection gate G1 as shown in figure 2. Doping profile modelling can affect transport through changes in the internal fields present in space-charge layers and through manipulation of the quasi-neutral fields present in graded-doping regions. A graded implantation for the photodiode can reduce the electron transit time since collection times are fairly rapid for mobile charge introduced in those regions. However, it could be extremely difficult to achieve such a profile. A multi-implant device with a staircase approximation to a graded pinned-buried photodetector is, therefore, used to reduce the readout time.

To achieve a high-speed detection, with essentially zero frame-to-frame lag, graded potential steps are created in the photodetector by variation of the doping concentration of implants. The concept of the charge readout time in a photodetector with multiple implants with a thermal diffusion model was initially developed [4]. According to this model the photodetector with three N-type detector implants is made up of three constant potential regions, each with an effective L_{eff} separated by a step potential of about 0.5 V. The effective photodetector charge readout time is estimated

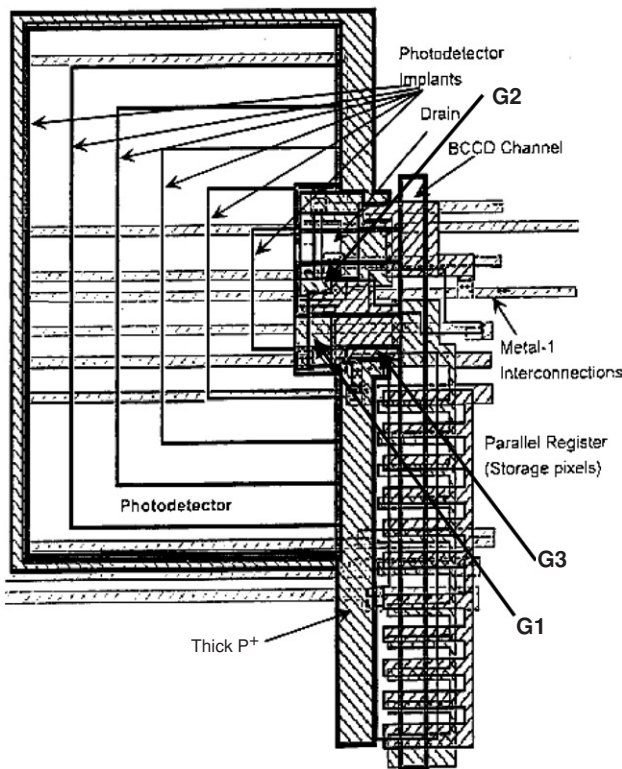


Figure 1. The micropixel design of an ultra-high frame rate burst image sensor.

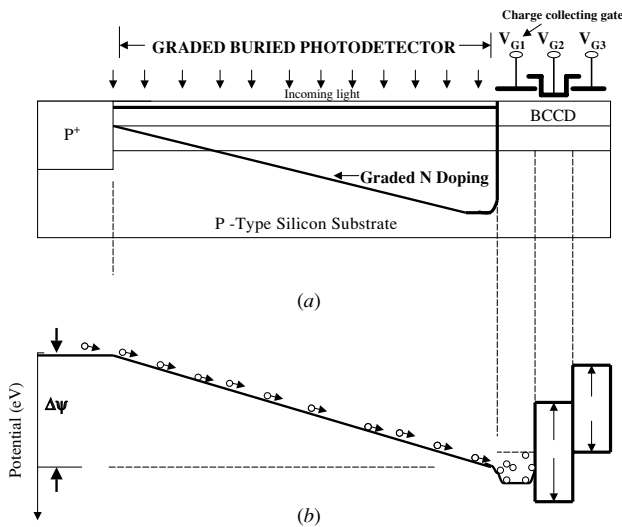


Figure 2. A schematic of the graded photodiode, where electrons are mostly drifted to the collecting gate.

as the thermal diffusion decay time or the transit time in the longest constant potential region plus an effective charge transfer between these regions. This model does not take into account the area or initial charge of an individual implant and the effective diffusion lengths for electrons closer and farther to the collection gate in the same implantation region. A charge transfer model that implements individual sections in the photodiode for a three-implant photodetector was reported earlier [5]. However, with only three implants it is not possible to achieve the required frame rate. Many more implants in the

photodiode are, therefore, necessary to speed up the charge transfer rate.

The present work describes a more generalized thermal diffusion model in an n -implant case. The model takes into account the initial photo-generated charge on each individual implant and the effective diffusion lengths of all electrons by dividing each implanted area into smaller sections or subsections. The design symmetry of each potential step was also considered for symmetrical designs. Even though the model can analyse a large number of implants the electron transit time in a model seven-implant photodiode is considered and compared with that of single-implant and three-implant cases previously developed.

2. Theoretical analysis

In a multi-implant setting, thermal diffusion and fringing field drift govern the electron motion in a photodetector. Introducing the current density relation into a continuity equation and solving the partial differential equation the effect of thermal diffusion was studied. The solution is given by [6]

$$Q(t) = \frac{8}{\pi^2} Q(0) \exp\left(-\frac{\pi^2 D_n t}{4L^2}\right) \quad (1)$$

where $Q(t)$ is the charge at time t , $Q(0)$ is the initial charge, L is the diffusion length, D_n is the diffusion coefficient and τ is the diffusion time constant represented by $4L^2/\pi^2 D_n$. It can be seen from equation (1) that the charge decreases exponentially with time from its initial value. The diffusion coefficient D_n is related to the electron mobility μ_n [7]. Since the time constant of the diffusion mechanism is inversely proportional to D_n and directly proportional to the square of the diffusion length, for a high-speed photodetector L should be small and D_n should be large. A multi-implant photodiode, therefore, reduces the charge readout time.

The cross-sectional view of an n - N -type-implant pinned-buried photodetector is shown in figure 3(a). The implant concentration N_1 is the BCCD implant plus the first photodetector implant. N_2 is N_1 plus the second photodetector implant. N_3 is N_2 plus the third photodetector implant and so on for the n - N implant. These implants result in an approximation to a graded potential profile along the photodetector as shown in figure 3(b). The potential profile divides the photodetector into n sections where section-2 acts as a charge sink for section-1, section-3 acts as a charge sink for section-2 and so on. Finally, the potential well under the charge-collecting gate acts as a sink for the charge collected by the photodetector. The effective transit length L was computed by subtracting the length δl due to fringing fields from the physical length L_0 of the implanted region as shown in figure 3(b). The transit time of the electrons for δl has been neglected as the electrons pass over a potential step. The image acquisition cycle is the most important cycle of the imager; during this cycle the charge signal is detected by the photodetector and is transferred in series into the registers for detection of successive frames [4].

The layout of the seven- N -type-implant pinned-buried photodetector ($100 \mu\text{m} \times 52 \mu\text{m}$) is shown in figure 4, where the detailed outline of the individual areas in the seven-implant case is specified. This figure can be generalized to obtain the

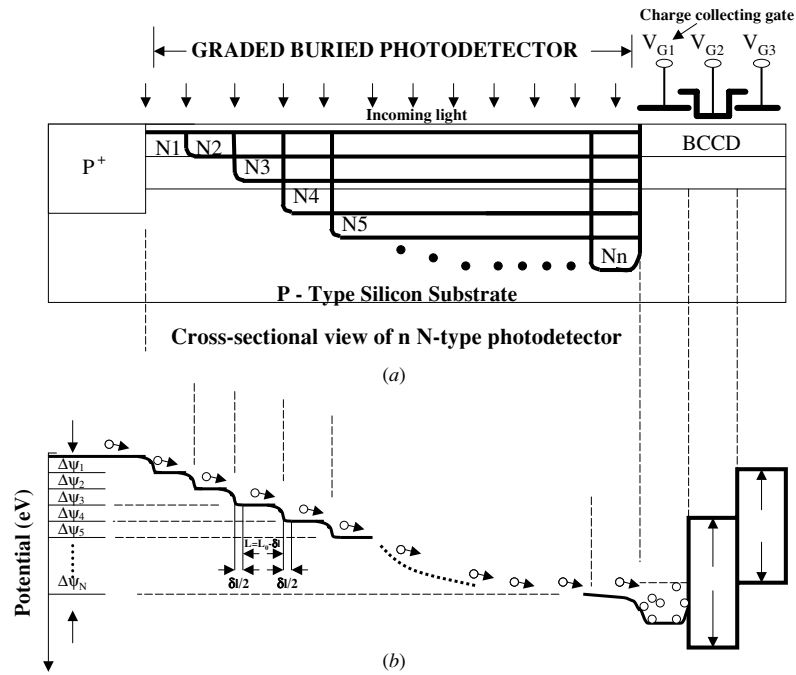


Figure 3. The cross-sectional view of the *n*-N-type-implant photodetector: (a) graded potential profile and operation and (b) the length δl represents the distance electron drifts due to the fringing field.

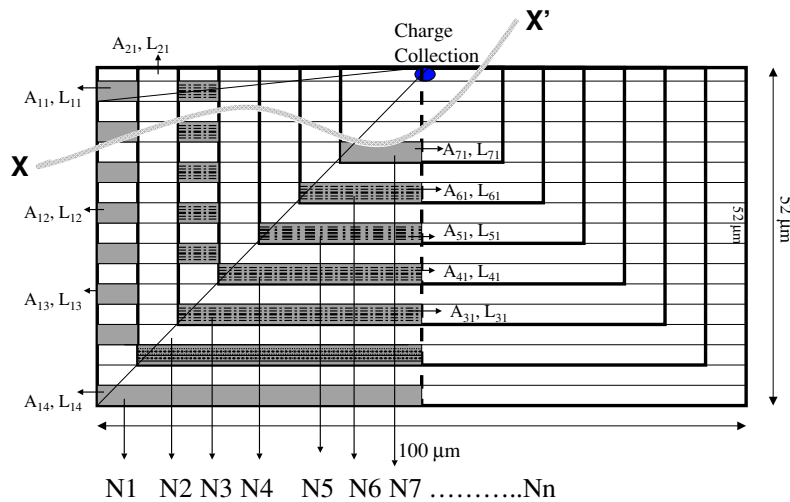


Figure 4. The layout of a seven-N-type-implant pinned-buried photodetectors shows different implantation regions and distribution of small areas.

layout for the *n*-N-implant photodetector. The curve *X*–*X'* represent the cross-section of the photodiode. The total area of the photodiode is *A* and *A*₁, *A*₂, *A*₃ . . . *A*_{*n*} are the areas of the implant regions. The charge transfer in a photodetector takes place from the entire area. To include charge transfer from different portions of the detector it is more accurate to divide the entire photodetector area into small areas. Thus, for simplicity and accuracy the entire photodetector area has been divided into small rectangular areas to avoid any overlapping areas as shown in figure 4.

The implant area *A*₁ is further divided into *p* number of small sections with an area of *A*_{1*i*} each. Similarly, the implant areas *A*₂, *A*₃, . . . *A*_{*n*} are divided into *q*, *r*, . . . *m* number of small sections with the areas of *A*_{2*j*}, *A*_{3*k*} . . . *A*_{*n**m*}, respectively.

The total charge in the photodetector at any time *t* can be obtained by the superposition of charges in all small sections at time *t*. Mathematically the charge at time *t*, *Q*(*t*), is represented as

$$\begin{aligned}
 Q(t) = & \frac{8Q(0)}{\pi^2 A} \left[\sum_{i=1}^p A_{1i} \exp\left(-\frac{\pi^2 D_{1n} t}{4L_{1i}^2}\right) \right. \\
 & + \sum_{j=1}^q A_{2j} \exp\left(-\frac{\pi^2 D_{2n} t}{4L_{2j}^2}\right) + \sum_{k=1}^r A_{3k} \exp\left(-\frac{\pi^2 D_{3n} t}{4L_{3k}^2}\right) \\
 & \left. + \dots + \sum_{m=1}^t A_{nm} \exp\left(-\frac{\pi^2 D_{nn} t}{4L_{nm}^2}\right) \right] \quad (2)
 \end{aligned}$$

where A_{1i} , A_{2j} , A_{3k} and A_{nm} are the i th, j th, k th and m th areas of the implantation for the regions A_1 , A_2 , A_3 and A_n , respectively.

D_{1n} , D_{2n} , D_{3n} and D_{nn} are the electron diffusion coefficients of the implant regions A_1 , A_2 , A_3 and A_n , respectively.

L_{1i} , L_{2j} , L_{3k} and L_{nm} are the effective maximum diffusion lengths of electrons in the i th, j th, k th and m th areas of the implant regions A_1 , A_2 , A_3 and A_n , respectively.

The dimension of the small areas in each implanted region is in the order of $6.25 \mu\text{m} \times 2.5 \mu\text{m}$ and different implantation regions of the seven-implant photodetector, therefore, have different number of these small areas. In figure 4 the symmetry in design reduces computation requirements for the model. However, if the layout of the photodiode is asymmetrical to optimize the quantum efficiency all the different areas need to be considered.

3. Results and discussion

Three different photodetector designs were considered to implement the present model to compute the charge transfer characteristics. In the first case a single-N-type-implant photodetector ($70 \mu\text{m} \times 45 \mu\text{m}$) was modelled where N was $1.4 \times 10^{17} \text{cm}^{-3}$. The corresponding electron mobility and diffusion coefficient were $700 \text{cm}^2 \text{V}^{-1} \text{s}^{-1}$ and $18.145 \text{cm}^2 \text{s}^{-1}$, respectively. The second case was a three-implant photodetector with the same dimensions as the single implant case. The doping concentrations were $N_1 \approx 1.4 \times 10^{17} \text{cm}^{-3}$, $N_2 \approx 2.6 \times 10^{17} \text{cm}^{-3}$ and $N_3 \approx 3.6 \times 10^{17} \text{cm}^{-3}$. The corresponding electron mobilities for the three concentrations were $\mu_{1n} \approx 700 \text{cm}^2 \text{V}^{-1} \text{s}^{-1}$, $\mu_{2n} \approx 600 \text{cm}^2 \text{V}^{-1} \text{s}^{-1}$, $\mu_{3n} \approx 500 \text{cm}^2 \text{V}^{-1} \text{s}^{-1}$, respectively. These mobilities give three different diffusion coefficients $D_{1n} \approx 18.145 \text{cm}^2 \text{s}^{-1}$, $D_{2n} \approx 15.576 \text{cm}^2 \text{s}^{-1}$ and $D_{3n} \approx 12.994 \text{cm}^2 \text{s}^{-1}$ for the three different implant regions. The effective maximum diffusion length of each section was computed by taking into account the fringing field drift [4]. The third case was the seven-implant photodetector (figure 3) where the doping concentrations were varied from $N_1 \approx 1.4 \times 10^{17} \text{cm}^{-3}$ to $N_7 \approx 3.6 \times 10^{17} \text{cm}^{-3}$ by equal increments. Therefore, the corresponding mobility values ranged from $\mu_{1n} \approx 700 \text{cm}^2 \text{V}^{-1} \text{s}^{-1}$ to $\mu_{7n} \approx 500 \text{cm}^2 \text{V}^{-1} \text{s}^{-1}$ and the diffusion coefficients were determined accordingly. Since the difference in the doping concentration between two adjacent implants reduced, the fringing fields were also scaled down. These modifications need to be incorporated in the model for n -implant photodiodes.

Figure 5 shows the comparison of electron transfer characteristics for the single-implant, three-implant and seven-N-type-implant photodetectors after the uniform illumination intensity corresponding to 20 000 electrons is turned off at $t = 0$. It can be seen that the charge readout time for the three-N-type-implant photodetector is much smaller than the one-N-type-implant photodetector. The number of electrons transferred from a small section to the collecting gate at time t depends on its initial number of electrons and the maximum effective diffusion length or location from the collecting gate. Transfer of electrons closer to the collecting gate takes less time, whereas transfer of electrons from the periphery of the

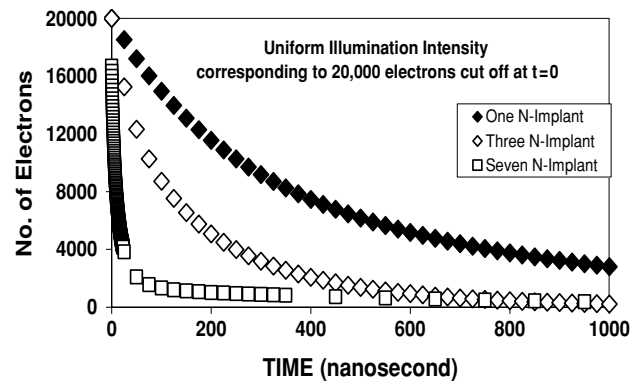


Figure 5. The comparison between electron transfer characteristics for the single-implant, three-implant and seven-N-type-implant photodetectors after the uniform illumination intensity corresponding to 20 000 electrons is turned off at $t = 0$.

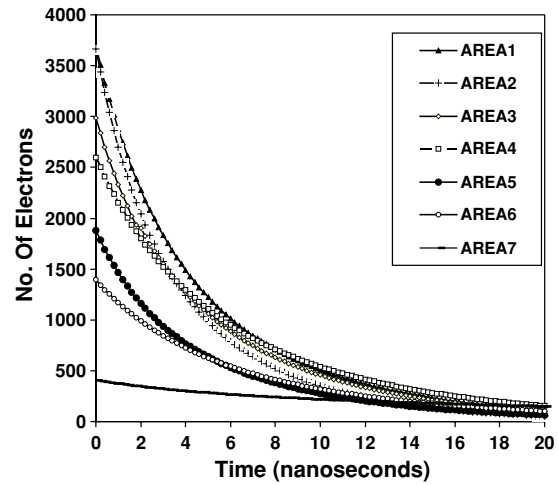


Figure 6. Available number of electrons in each individual implanted region as a function of time after the uniform illumination intensity corresponding to 20 000 electrons is turned off at $t = 0$.

photodetector takes longer time. On average, the electron transfer mechanism from the implant region A_1 is the slowest and the fastest from the implant region A_n . The total number of electrons in the photodetector is obtained by the superposition of the contribution of the number of electrons from each small section. For 90% electron transfer the readout time for the single-implant detector, three-implant detector and seven-implant detector is more than 1000 ns, about 500 ns and 50 ns, respectively.

Figure 6 shows the available number of electrons in each individual implanted region in the photodetector as a function of time after the uniform illumination intensity corresponding to 20 000 electrons is turned off at $t = 0$. Considering uniform generation of photocarriers the distribution is the function of an individual area of a particular implanted region. The electron transfer from each implant region depends on the initial number of electrons and the maximum distance the electron has to travel due to diffusion (flat surfaces in figure 3). The readout time for 90% electron transfer from each implant region is different. For the photodetector as a whole, for 90% of electrons transfer the readout time is about 50 ns considering the superposition of each individual region.

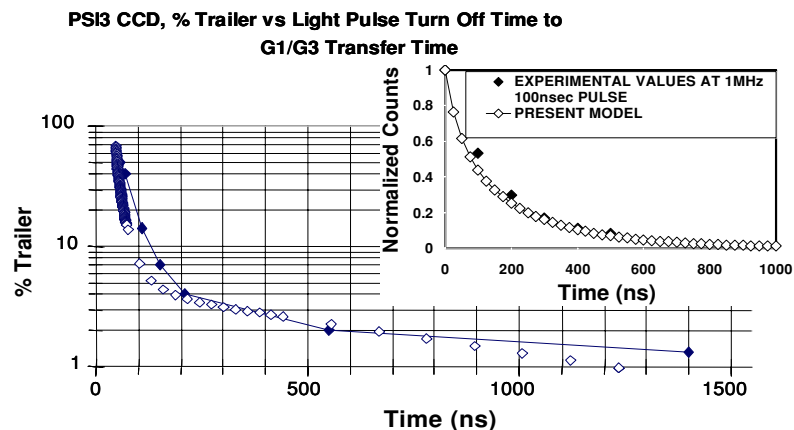


Figure 7. The comparison between charge readout values obtained by the present model and the experimental charge readout values for a seven-implant photodiode (open diamonds indicate the calculated intensity whereas closed diamonds indicate the experimentally measured intensity). The inset shows the comparison with the three-implant case.

A high burst rate CCD capable of imaging at 1–5 million frames s^{-1} has been published [8]. The charge readout comparison between the experimental results (1 MHz and 100 ns pulse) [8] and the results obtained by using the present model is shown in figure 7 where we have plotted the percentage of charge transfer as a function of time for seven-implant photodiodes. Open diamonds in figure 7 indicate the calculated intensity of the trailing image whereas solid diamonds show the experimental percentage trailer as a function of the time between the end of the light pulse and transfer of the photoelectrons in a seven-implant photodiode. It can be seen that for 90% electron transfer the experimentally observed readout time is approximately 90 ns and the readout time obtained by the present model is about 70 ns to G1/G3 gates. The inset in figure 7 shows the comparison of the present model with that of the experimental results obtained from a three-implant case. The significant decrease in the readout time for the seven-implant case was noticed. The readout time is a function of the doping profile distribution in the photodiode. By increasing n (number of regions) in an n -implant photodiode the transit time can be decreased further. When n is sufficiently high the stair case potential distribution will be a smooth profile and the electron transport will take place mostly by drift due to the fringing field in the photodiode as shown in figure 2. A linearly graded implantation for the photodiode can therefore reduce the electron transit time further. However, it could be extremely difficult to achieve such a profile and also increase the number of processing steps.

4. Conclusions

In conclusion, a thermal diffusion model has been developed for n -N-type-implant pinned-buried photodetector. This model takes into account the initial charge of each implant and the effective length of the far and near electron. The model was used to estimate the charge transfer in three-implant and seven-implant photodiodes. The model considers the fringing field effect at the interface of two adjacent

implants. The results obtained by this model agree with the experimental values when compared in the case of a three-implant photodiode. By increasing the number of implants the transit time can be decreased further. However, many mask steps may be necessary but the staircase potential distribution will be a smooth graded profile and electron transport will take place mostly by drift due to the built-in fringing field in the photodiode.

Acknowledgments

The authors wish to acknowledge Dr J L Lowrance of Princeton Scientific Instruments, and Dr P K Swain of Sarnoff Corporation, NJ, for experimental data. The financial support from New Jersey Commission and National Science Foundation (Award ECS-0140584) is acknowledged.

References

- [1] Kosonocky W F and Lowrance J L 1994 High frame rate CCD imager *US Patent* 5355165
- [2] Kosonocky W *et al* 1996 360×360 -Element very high frame-rate burst-image sensor *Proc. 1996 IEEE Int. Solid State Circuits Conf. (San Francisco, CA)* pp 182–3
- [3] Reich R K, O'Mara D M, Young D J, Loomis A H, Rathman D D, Craig D M, Watson S A, Ulibarri M D and Kosicki B B 2001 High-fill-factor, burst-frame-rate charge-coupled device *IEDM Technical Digest* p 567
- [4] Yang G 1996 Design, process, and performance simulation of a 360×360 -element very high frame-rate Burst-image sensor *PhD Dissertation*, New Jersey Institute of Technology, Newark
- [5] Jarwal R K, Misra D and Lawrance J L 2001 Charge transfer in a multi-implant pinned-buried photodetector *IEEE Trans. Electron Devices* **48** 858–62
- [6] Carnes J E, Kosonocky W F and Ramberg E G 1972 Free charge transfer in charge coupled devices *IEEE Trans. Electron Devices* **19** 798–802
- [7] Sze S M 1985 *Semiconductor Devices Physics and Technology* (New York: Wiley)
- [8] Swain P K *et al* 2001 *IEEE Workshop on Charge-Coupled Devices and Advanced Image Sensors (Lake Tahoe, Nevada, 7–9 June 2001)*